NIPES

Journal of Materials Engineering, Structures and Computation

Journal homepage: www.nipesjournals.org.ng

Bioactivity Assessment of Multi-doped Hydroxyapatite Nanoparticles $Ca_{9.2}Mg_{0.8}Cu_{0.001}(PO_4)_{5.9}(CO_3)_{0.06}(SiO_4)_{0.04}(OH)_{2.0}$ from Ion Release and Morphology Correlators

Iliya Ezekiel[a], Edema O. G.[b,*] and Akinbolusere, A. O[b].

[a]*Department of Ceramics Technology, School of Applied Sciences and Technology, Auchi Polytechnic, Auchi*
[b]*Department of Physical Science Laboratory Technology, School of Applied Sciences and Technology, Auchi Polytechnic, Auchi*

ARTICLE INFORMATION

Article history:
Received 02 April 2023
Revised 16 May 2023
Accepted 18 May 2023
Available online 12 June 2023

Keywords:
Carbonated hydroxyapatite, ICP-OES, FE-SEM, bioactivity

https://doi.org/10.5281/zenodo.8027697

ABSTRACT

This work focused on the bioactivity study of carbonated hydroxyapatite ($Ca_{10}(PO_4)_6(CO_3)_6(OH)_2$) and multi-doped ($Mg^{2+}$, Si^{4+} and Cu^{2+}) carbonated hydroxyapatite ($Ca_{10-x/2-a-b}Mg_aCu_b(PO_4)_{6-x-y}(CO_3)_x(SiO_4)_y(OH)_{2-y}$).The nanopowders were cylindrically pressed into pellet and sintered at 800 °C and transferred into 30 mL vial Simulated Body Fluid (SBF) media for bioactivity analysis. Materials characterization tools such as X-ray fluorescence (XRF), Field Emission Scanning Electron Microscope (FES-SEM) and Inductive Coupled Plasma Optical Emission Spectroscopy (ICP-OES) were used for elemental composition, ion release and morphology studies respectively. The obtained result indicate that the multi-doped sample tagged MSC-CHAp shows a superior bioactivity with visible apatite layer compared to the control sample (CHAp). This improved bone-like apatite layer was due to lower ion release in the solution and higher participatory activity of Ca^{2+} and PO_3^{4-} on the surface of the pellets

1. Introduction

A key component of bioceramics employed in bone tissue engineering and regeneration is calcium phosphate (CaP) ceramics. This category of bone graft substitute (BGS) have found myriad of applications in drug delivery systems, CaP cements, coatings and scaffold archetypes [1]. Typically, hydroxyapatite (Hap), β-tricalcium phosphate (β-TCP) and biphasic calcium phosphates constitute the most used CaP bioceramics. The chemical structure of Hap and β-TCP composed of $Ca_{10(I)(II)}(PO_4)_6(OH)_2$ and $Ca_3(PO_4)_2$ respectively [2]. Biphasic CaP ceramics comprised of ratios of HA and β-TCP. In addition, monotite ($CaHPO_4$) is an important and precursory phase of these dominant CaP materials. $CaHPO_4$ has greater *in vivo* resorbability in comparison to CaP cements and better solubility than β-TCP and Hap in aqueous solutions at the physiological pH [3].

The mammalian hard tissue contains elements like Ca, Mg, Cu and Si that play a vital role in bone formation. Calcium is a chief content found in bones, teeth and skull, deficit of which leads to several terminal conditions. Magnesium is essential for the regulation of bone growth, repair and preservation while silicon is the required element for skeletal development, and its deficit can cause skull deformation [4]. Copper (Cu) has been reported to be able to stimulate vascularization/angiogenesis, which is critical for regeneration of vascularized tissue in tissue engineering [5].

Several literature reports have been dedicated to preparation and substitution of carbonated hydroxyapatite bioceramics. In this research a correlation studies of ICP-OES and FE-SEM were deployed in order to ascertain the apatite activity. The goal is to establish that ion release triggered from bioactivity interaction in SBF solution can be linked to the morphology of biomaterials.

2. Materials and Method

2.1 Materials Preparation

The synthesized carbonated hydroxyapatite $Ca_{10}(PO_4)_6(CO_3)_6(OH)_2$ (CHAp) powders by direct pouring nanoemulsion method was adopted in our earlier work [6]. In our previous research we established the reliability of the synthetic CHAp nanopowders produced using X-ray diffraction (XRD), Fourier transform infrared (FTIR) spectroscopy, field-emission scanning electron microscopy (FESEM), X-ray fluorescence (XRF), carbon-hydrogen–nitrogen analysis (CHN), *Brunauer–Emmett–Teller* (BET) method, transmission electron microscopy (TEM).

2.2 Pelletizing and sintering carbonated HA

The pelletizing and sintering of the CHAp and multi-substituted CHAp samples. The powders samples were pelletized into compact cylindrical solid by dry pressing using a hydraulic hand press machine and stainless steel mould with a diameter of 13 mm. To prepare each pellet, 0.5 g of the as-prepared powder sample was weighed in a scale and transferred carefully into the shaft of the mould steel sleeve. A uniaxial pressure of 50 MPa was applied to the powders in sandwiched between the core dies by the push press and held for 2 minutes to ensures consistency of compaction. Later, the pressure was released and the mould overturned to push out the pellet slowly through the shaft of the steel sleeve. The dry pressed pellet was then sintered at 800 ˚C at a rate of 5 ˚C $min.^{-1}$ and soaking time of 120 minutes using a Lenton box furnace under air atmosphere. Next, the properties of the sintered pellets were analyzed.

2.3 Materials characterization

The following characterization tools were employed in analysing the sintered pellets of CHAp:

- ✓ X-ray diffraction (XRD)
- ✓ X-ray fluorescence (XRF),
- ✓ Field Emission Scanning Electron Microscope (FESEM),
- ✓ Inductive Coupled Plasma Optical Emission Spectroscopy (ICP-OES).

2.3.1 X-Ray Diffraction (XRD)

XRD in the interval of angles $20° \leq (2\theta) \leq 60°$ (Cu Kα radiation; Bruker Advanced X-ray Solution D8, Bremen, Germany) was used to determine the lattice parameter, crystallite size, and phase of powders. The X'Pert High Score Plus software was used. Inferred patterns were matched with the International Center for Diffraction Data with file number 00-009-0432 designated for standard HA to estimate the phase type and size of crystals. The crystallite size was calculated by XRD through Scherrer's equation below [7]:

$$L = \frac{k\lambda}{\beta_{1/2}\cos\theta}$$

where *L* refers to the crystallite size (nm), λ (1.5404 Ǻ) refers to the wavelength of Cu Kα radiation, β) refers to the full width at half maximum (radian), θ is the diffraction angle (degrees), and k is the boarding constant (0.94). In this regard, distinct diffraction peaks of (002), (211), and (300) with high intensities, were selected for evaluation. Rietveld refinement was conducted on the chemical compound to confirm the effect of carbonate and multi-doped ions on the apatite structure.

2.3.1 XRF

XRF spectrometer operations involves analysis of individual quantity of the elements present in samples. XRF spectrometry working mechanism encompasses the emission of x-ray photon beam that is incident upon the atoms of a sample. The interface of the primary x-ray beam with the atoms of the sample excites the electrons, causing some electrons exiting their orbit. The atomic concentration of elements in the samples was quantified by X-ray Fluorescence Spectrometer (XRF: Rigaku Rix 3000, Japan).

2.3.2 FESEM

FE-SEM provides topographic images of surface or fractured samples microscopically at the electron level. This is achieved by releasing and accelerating high-energy beam of electrons in a raster scan pattern from field emission gun sources [8]. The morphology and surface properties of the samples were studied using Field Emission Scanning Electron Microscope (FESEM: Zeiss Supra 35VP, USA). In addition, the bioactivity observed using FE-SEM in the form of apatite film on the sintered pellets immersed via SBF media. The samples were prepared by sputtering of gold coat on samples to form a surface coat. The surface coat ensured actual surface conductivity of the samples that avoids image flaws.

2.3.3 ICP-OES

ICP-OES are designed to determine the composition of a wide variety of materials, with excellent sensitivity. The ICP-Optical Emission Spectrometer (ICP-OES), sometimes referred to as an ICP-Atomic Emission Spectrometer (ICP-AES), separates the light emitted from the plasma into its discrete component wavelengths using a diffraction grating. Each element in the periodic table has its own distinct set of emission wavelengths. Inductive Coupled Plasma Optical Emission Spectroscopy (ICP-OES: Perkin Elmer Optima 7300 DV, USA) was employed in ion release as its correlate to the morphological investigation.

2.3.4 *In vitro* Bioactivity Assessment

In order to ascertain the bioactivity of the CHAp sample in vitro test was conducted in SBF solution in agreement to works by Kokubo and Takadama [9]. The pellets were dropped in (Vs = 30 mL) vial containing SBF solution and pH was recorded weekly using a pH meter. Volume of the required SBF solution for each sintered pellet was assessed as shown in Eq. 1. [9].

$$Vs = Sa / 10 \quad (1)$$

wherein Vs is the volume of the SBF in mL and Sa is the apparent surface area of the specimen in mm^2. The Sa was determined by the surface area of the cylindrical pellet shape by Eq. 2.

$$Sa = 2\pi r^2 + 2\pi h \quad (2)$$

where r is the radius and h the height or thickness in mm of the pellets.

Then FESEM assessment of apatite layer and surface morphology of the samples was conducted at 37^{o}C (pH = 7.4) after soaking (7, 14 and 21 days) in SBF solution. The concentration of ions in the leachate of SBF media was measured by ICP-OES. Analysis of the concentrations of ion release present was measured at wavelength at the detectable wavelength in nm.

2.3.5 Preparation of Simulated Body Fluid (SBF)

To prepare 1L solution of SBF, the following reagents listed sequentially in Table 3.4 were strictly followed and only water in agreement with ISO 3696:1987, grade two, was used.

Table 1. Chemical reagents for the preparation of 1L SBF solution [9].

Order	Reagent	Amount	Purity (%)	Formula weight ($gmol^{-1}$)
#1	NaCl	8.035 g	99.5	58.4430
#2	$NaHCO_3$	0.355 g	99.5	84.0068
#3	KCl	0.225 g	99.5	74.5515

#4	$K_2HPO_4 \cdot 3H_2O$	0.231g	99.0	228.2220
#5	$MgCl_2 \cdot 6H_2O$	0.311 g	98.0	203.3034
#6	1.0 M HCl	39 mL	–	–
#7	$CaCl_2$ or $CaCl_2 \cdot 2H_2O$	0.292 g	95.0	110.9848
#8	Na_2SO4	0.072 g	99.0	142,0428
#9	Tris $(HOCH_2)_3CNH_2$	6.118 g	99.0	121.1356
#10	1.0 M HCl	0-5 mL	–	–

The procedure began by pouring 700 mL of ion-exchanged and distilled water into a smooth surface 1 L plastic beaker with a magnetic bar. The plastic was then submerged in a bigger glass beaker containing water and the temperature was maintained at 36.5 ± 1.5 °C by control heating while stirring on the magnetic stirrer. In the order of arrangement from #1 to #8 (Table 1) the reagents were dissolved in distilled water one at a time accordingly.
The hygroscopic reagents (#3, #4, #5 and #8) were rapidly weighed and dissolved and the electrode of the pH meter was put into the solution. The pH of the solution was observed to be 2.0 ± 1.0 and a stringent temperature of 36.5 ± 0.5 °C was maintained before the introduction of reagent #9. Gradually reagent #9 was dissolved in the solution and upon completion, a pH of 7.45 at a control temperature of 36.5 ± 0.5 °C was noted. To lower the pH to 7.42, reagent #10 was introduced in drops and the electrode removed as the solution was transferred into a 1 L volumetric flask. Then, distilled water was added to increase the 700 to 1000 mL and covered with plastic film. The final product was kept at 20 °C and labeled for use within 1 month.

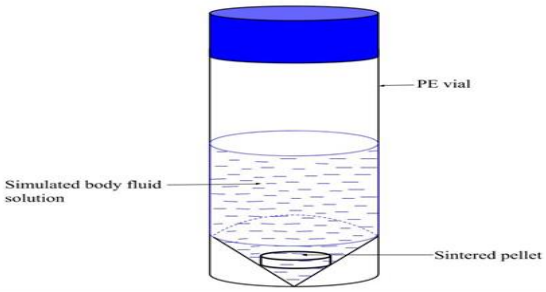

Figure 1. Graphical representation of sintered multi-doped carbonated HA immersed into SBF solution

ICP-OES refers to trace-amount, elemental analysis that utilizes the emission spectra of a sample to identify and quantify the elements present. The samples are introduced into the plasma in a process that desolvates, ionises, and excites the same samples. Composition in the form the sample elements are assessed by their unique emission lines and measured intensity of the given lines. The leachate was converted into fine aerosol vapour, which allowed for transportation via a nebulizer with an argon stream into a plasmatic burner. The concentrations of the samples were measured at wavelengths of Ca^{2+}; 393.366, P^{5+}; 177.499, Mg^{2+}; 279.553 and Cu^{2+}; 324.754 nm respectively.

3. Results and Discussion

3.1 X-Ray Diffraction (XRD) Analysis

3.1 XRF

The XRF result indicate the presence of typical composition of bone graft inorganic constituent in CHAp and MSC-CHAp. Table 1 shows the theoretical phase model composition of natural bone adopted for CHAp and hypothetical (multi-doped CHAp) MSC-CHAp reflecting both Ca/P ratios respectively. The phase formula elements in both samples were selected in accordance to the quantity found in human bone. The result from Table 2 shows the experimental XRF data closely in agreement with the theoretical model. It is worth noting that CHN/S was employ to ascertain the CO_3^{2-} content in both samples. The decrease trend of the theoretical phase formula's Ca/P ratio of

MSC-CHAp (1.56) in comparison to CHAp (1.68) was observed in the experimental result (1.90 from 1.93). The decrease can be attributed to largely the multi-substitution activities at Ca^{2+} site.

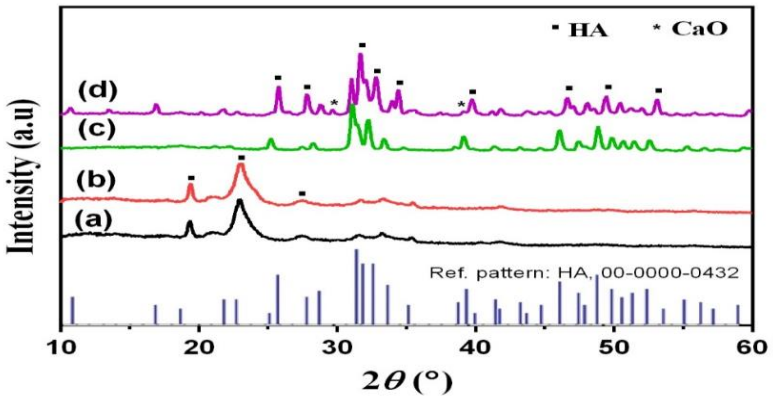

Figure 2. XRD pattern of as synthesize (a) CHAp (b) MSC-CHAp (c) sintered) CHAp (d) sintered MSC-CHA

Table 2. Theoretical phase formula and lattice parameter for CHAp and MSC-CHAp

Acronym	**Phase formula**	**Ca/P**
CHAp	$Ca_{9.970}(PO_4)_{5.940}(CO_3)_{0.060}(OH)_{2.00}$	1.68
MSC-CHAp	$Ca_{9.2095}Mg_{0.7596}Cu_{0.0009}(PO_4)_{5.9029}(CO_3)_{0.060}(SiO_4)_{0.0371}(OH)_{1.963}$	1.56

Lattice parameter							
	Lattice constant			$d_{Scherer}$	**Lattice (ε)**	**FWHM**	X_C**%**
	***a* (Å)**	***c* (Å)**	***c*/*a***	**(nm)** [x]	**(%)** [y]	**(º)**	**(%)** [z]
CHAp	9.417	6.879	0.730	34.68	0.330	0.245	97.96
MSC-CHAp	9.386	6.853	0.730	22.75	0.519	0.390	61.53

Table 3. XRF elemental composition from synthesized CHAp and MSC-CHAp

Element ≠CHN/S data	**Compositions (wt. %)**	
	CHAp	**MSC-CHAp**
Mg	-	0.2501
Si	-	0.0418
Cu	-	0.0043
Ca	27.4799	25.2505
P	14.2151	13.3232
O	58.3050	61.1301
(CO_3) ≠	3.2200	3.3500
Ca/P	1.9300	1.9000

3.2 FESEM

The apatite development is mainly dependent on interaction of the identical anionic-cationic constituent of SBF media with a negatively charged surface of HAp. Apatite minerals are made at the pellets surface when deprived Ca^{2+} and rich Ca^{2+} at surface of the pellets interact with PO_4^{2-} from the SBF solution [10]. In this study, apatite layer formed in the control CHAp and MSC-CHAp pellet at 800 (Fig. 3 (a) and (b)) after soaking for 14 days in SBF solution exhibited an early formation of apatite crystals. Larger non dispersed flower-like apatite was observed in CHAp and bone-like apatite layer further increased in MSC-CHAp.

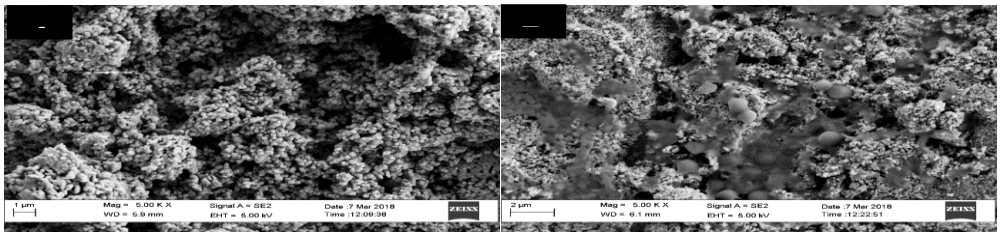

Figure 3. FE-SEM micrograph (a) CHAp and (b) MSC-CHAp showing bioactivity morphology

3.3 ICP-OES

The ion release shows the regulatory state in dissolution of CaP bioceramics owing to the mobility of ions into the SBF solution or by occurring on the crystal surfaces. Consequently, the SBF medium hydrolyses ($Ca_2(HPO_4)(OH)_2$) as it becomes more acidic thus discharging more ions and hydrolyses less in an alkaline state [11]. The sintered control CHAp and multi-substituted MSC-CHAp presents surface abnormalities and structural defects inside and on the surface bulk of CaP crystals. Therefore, this generates dissolution nuclei that enable the rate of ion release. Fig. 2(a) indicated an increase in Ca^{2+} release after 7 days of immersion into SBF solution which then stabilized after 14 and 21 days for the MSC-CHAp samples. The control CHAp displayed the highest Ca^{2+} release across all soaking days. Although after 14 days, there is a drop in Ca^{2+} release. This is can be attributed to the absent of other ionic dopants. The comparatively MSC-CHAp Ca^{2+} release is an indication of the interference from other ions in particular Si^{4+} reported of forming amorphous layer hence inhibiting the release of Ca^{2+} [12].

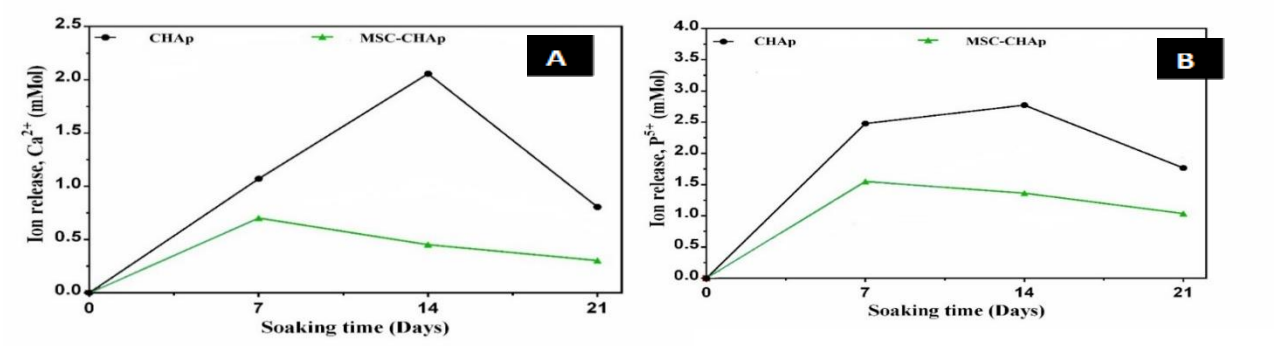

Figure 4. ICP-OES ion release analysis (a) CHAp and (b) MSC-CHAp.

In Figure 4(b), the phosphorus release in the samples increased until saturation after 14 days where it gradually stabilizes to day 21. The control CHAp indicated a higher P release in contrast to the MSC-CHAp sample with relatively low P release. The lesser P concentration in the SBF can signify that the active participation of P in apatite development was greater than dissolution rate [13]. The outcome from this research indicate the lowest P ion release in MSC-CHAp that implies a vigorous involvement of this ion in apatite formation compared to the control sample.

4. Conclusion

Bone-like carbonated hydroxyapatite nanopowders synthesized were compacted into pellet and sintered for ICP-OES/FE-SEM correlational studies of bioactivity. Successful experimental composition and dopants inclusions in CHAp and MSC-CHAp were confirmed using XRF. The ICP-OES results lower release in Ca^{2+} and P^{5+} ion in both multi-substituted samples, indicating higher participatory role in apatite layer formation as reflected on the FE-SEM micrograph. The *In vitro* bioactivity tests of the control sample and multi-substituent sample suggested a comparatively enhanced bioactivity of multi-substituent sample due to lower ion releases and higher participatory activities. Over all, the results indicate that this improved bioactivity could have promising applications in drug delivery systems, bone and tissue engineering.

References

[1] Despoina Xidaki, Panagiota Agrafioti, Dimitra Diomatari, Archontia Kaminari, Eleftherios Tsalavoutas-Psarras, Polyxeni Alexiou, Vasilios Psycharis, Effie C. Tsilibary, Spyridon Silvestros and Marina Sagnou. (2018). Synthesis of Hydroxyapatite, β-Tricalcium Phosphate and Biphasic Calcium Phosphate Particles to Act as Local Delivery Carriers of Curcumin: Loading, Release and In Vitro Studies. Materials 11, 595.

[2] P. Wongwitwichot, J. Kaewsrichan, K. H. Chua, and B.H.I Ruszymah (2010). Comparison of TCP and TCP/HA hybrid scaffolds for osteoconductive activity. The open Biomedical Engineering Journal, 4: 279.

[3] Esmael Salimi and Jafar Javadpour (2012). Synthesis and Characterization of Nanoporous Monetite Which Can Be Applicable for Drug Carrier. Journal of Nanomaterials.
[4] R. Choudhary, S. Koppala and S. Swamiappan (2015). Bioactivity studies of calcium magnesium silicate prepared from egg shell waste by sol–gel combustion synthesis. Journal of Asian Ceramic Societies, 3: 173–177.
[5] N. Kong, K. Lin, H. Li and J. Chang (2014). Synergy effects of copper and silicon ions on stimulation of vascularization by copper-doped calcium silicate. J. Mater. Chem. B, 2: 1100.
[6] E. Iliya, S. R. Kasim, Y. M. Baba-ismail and M. N Ahmad-Fauzi (2018), Nanoemulsion synthesis of carbonated hydroxyapatite nanopowders: Effect of variant CO_3^{2-}/PO_4^{3-} molar ratios on phase, morphology, and bioactivity. Ceramics International, 44 (11): 13082-13089.
[7] A. J. Wagoner Johnson and B. A Herschler (2011). A review of the mechanical behavior of CaP and CaP/polymer composites for applications in bone replacement and repair. Acta Biomaterialia, 7(1), 16 - 30.
[8] A. Alyamani and O. M. Lemine (2012). FE-SEM Characterization of Some Nanomaterial. Ceramics International, 34 (5): 2082-2089.
[9] T. Kokubo and H. Takadama (2006). How useful is SBF in predicting in vivo bone bioactivity? Biomaterials, 27: 2907-2915.
[10] Mohamed Jamil, Fatima Abida, Zineb Hatim, Mostafa Elassfouri and Elhassan Gourri (2015). Effects of ions traces on the dissolution of bioceramics composed of hydroxyapatite and β-tricalcium phosphate. Mediterranean Journal of Chemistry, 4(1), 51- 58
[11] H. M. Kim, T. Himeno, M. Kawashita, T. Kokubo and T. Nakamura (2004). The mechanism of biomineralization of bone-like apatite on synthetic hydroxyapatite: an in vitro assessment. Journal of The Royal Society Interface, 1**:** 17-22.
[12] M. Latifi, M. Fathi, J. Varshosaz and N. Ghochaghi (2015). Mechanisms controlling cation release from sol-gel derived in situ apatite-silica nanocomposite powder. Ceramis Silikaty, 59 (1): 64 - 69.
[13] L. Xie, H. Yu, W. Yang, Z. Zhu and L. Yue (2016). Preparation, in vitro degradability, cytotoxicity, and in vivo biocompatibility of porous hydroxyapatite whisker-reinforced poly (L-lactide) biocomposite scaffolds. Journal of Biomaterials Science, Polymer Edition, 27: 505-528.

Appendix

Table 1. Chemical reagents for the preparation of 1L SBF solution [9].

Order	Reagent	Amount	Purity (%)	Formula weight ($gmol^{-1}$)
#1	NaCl	8.035 g	99.5	58.4430
#2	$NaHCO_3$	0.355 g	99.5	84.0068
#3	KCl	0.225 g	99.5	74.5515
#4	$K_2HPO_4 \cdot 3H_2O$	0.231g	99.0	228.2220
#5	$MgCl_2 \cdot 6H_2O$	0.311 g	98.0	203.3034
#6	1.0 M HCl	39 mL	–	–
#7	$CaCl_2$ or $CaCl_2 \cdot 2H_2O$	0.292 g	95.0	110.9848
#8	Na_2SO4	0.072 g	99.0	142,0428
#9	Tris $(HOCH_2)_3CNH_2$	6.118 g	99.0	121.1356
#10	1.0 M HCl	0-5 mL	–	–

Table 2. Theoretical phase formula and lattice parameter for CHAp and MSC-CHAp

Acronym	Phase formula	Ca/P
CHAp	$Ca_{9.970}(PO_4)_{5.940}(CO_3)_{0.060}(OH)_{2.00}$	1.68
MSC-CHAp	$Ca_{9.2095}Mg_{0.7596}Cu_{0.0009}(PO_4)_{5.9029}(CO_3)_{0.060}(SiO_4)_{0.0371}(OH)_{1.963}$	1.56

	Lattice parameter						
	Lattice constant			$d_{Scherer}$	Lattice (ε)	FWHM	X_C%
	***a* (Å)**	***c* (Å)**	***c*/*a***	**(nm)** [x]	**(%)** [y]	**(º)**	**(%)** [z]
CHAp	9.417	6.879	0.730	34.68	0.330	0.245	97.96
MSC-CHAp	9.386	6.853	0.730	22.75	0.519	0.390	61.53

Table 3. XRF elemental composition from synthesized CHAp and MSC-CHAp

Element	Compositions (wt. %)	
≠CHN/S data	**CHAp**	**MSC-CHAp**
Mg	-	0.2501
Si	-	0.0418
Cu	-	0.0043
Ca	27.4799	25.2505
P	14.2151	13.3232
O	58.3050	61.1301
(CO_3) ≠	3.2200	3.3500
Ca/P	1.9300	1.9000